Available online at www.sciencedirect.com

ScienceDirect

journal homepage: www.elsevier.com/locate/he

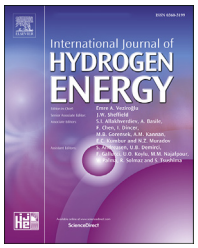

Functionalized carbon dots on TiO_2 for perovskite photovoltaics and stable photoanodes for water splitting

A. Ansón-Casaos [a,*], J. Hernández-Ferrer [a], L. Vallan [a], H. Xie [b], M. Lira-Cantú [b], A.M. Benito [a], W.K. Maser [a]

[a] Instituto de Carboquímica, ICB-CSIC, Miguel Luesma Castán 4, 50018 Zaragoza, Spain
[b] Catalan Institute of Nanoscience and Nanotechnology (ICN2), CSIC and Barcelona Institute of Science and Technology (BIST), Building ICN2, Campus UAB, Bellaterra, 08193 Barcelona, Spain

HIGHLIGHTS

- Fluorescent carbon dots (CDs) are synthesized bottom-up and modified chemically.
- Nitrogen-CDs increase the open circuit voltage in perovskite solar cells.
- Butyl-CDs improve the water splitting photocurrent of TiO_2 films by 125%.
- The CD/TiO_2 anodes are stable and show an extended light absorption range.

ARTICLE INFO

Article history:
Received 19 November 2019
Received in revised form
6 February 2020
Accepted 4 March 2020
Available online 1 April 2020

Keywords:
Titanium dioxide
Carbon nanoparticle
Solar energy
Renewable hydrogen
Sustainability

ABSTRACT

Various types of fluorescent carbon nanoparticles, often called carbon dots (CDs), are synthesized by different polycondensation methods: microwave irradiation, hydrothermal conditions or solution chemistry at ambient temperature with subsequent chemical functionalization. The CDs are deposited on TiO_2 films to be probed as electron transport layers in perovskite photovoltaics and the anode for photoelectrochemical water splitting. Nitrogen CDs, which do not contain oxygen, lead to an increase of around 50 mV in the open circuit voltage of perovskite solar cells. All the CD types produce an improved photocurrent in water splitting, particularly CDs that are functionalized with thiol groups and butyl chains. It is demonstrated that the modified electrode is stable under continuous operation. Other electrochemical characteristics of the electrode, such as the voltammogram shape, onset potentials and open circuit potentials, remain nearly unchanged upon the deposition of CDs. Only the incident photon to current conversion efficiency improves clearly, extending the absorption range by around 20 nm towards longer wavelengths. This study provides new data about mechanisms and electrode arrangements for improving the performance of n-type semiconductors in photovoltaic cells and photoelectrochemical hydrogen production.

* *Corresponding author.*
E-mail address: alanson@icb.csic.es (A. Ansón-Casaos).
https://doi.org/10.1016/j.ijhydene.2020.03.077

Introduction

Titanium dioxide has been widely studied in advanced oxidation processes, photovoltaics and electrochemical water splitting [1–4]. In particular, TiO_2 films have been utilized as electron transport layers in dye-sensitized and perovskite solar cells [2,4,5]. Similar layered configurations, in which TiO_2 behaves as the active phase, are typical in photoelectrochemical (PEC) water oxidation. Intense research efforts are being devoted to improve the performance of these systems [5–7].

The efficiency of TiO_2 photoanodes in electrochemical water splitting has been improved by many strategies, including metal nanoparticle deposition, cationic and anionic doping, and sensitization [1,8]. Currently applied ideas include the development of ordered porosity and core-shell structures [9–12], TiO_2 functionalization and hydrogenation [9,13], the control of phase junctions [10,14], cheap metal alloys as co-catalysts [15–17], plasmonic effects [18], and the design of tandem ensembles and cascade charge transfer pathways [19–21], among others. In addition, mixtures with carbon materials such as carbon nanotubes [22–25] and graphene [26–29] have been tried. More recently, it has been observed that carbon dots (CDs) on TiO_2 can lead to positive effects in reactions of photoassisted hydrogen generation. The family of CDs includes many types of fluorescent nanoparticles that are synthesized either by top-down methods, typically from graphite, or bottom-up processes from simple organics such as short chain acids and amines. Many of the CD forms have graphene structures in their cores, and are usually called graphene quantum dots. Some others do not present conjugated carbon chains, and are sometimes called polymer dots. The photoluminescence properties of CDs are determined by the synthesis method and can be tuned by functionalization with chemical groups that induce charge transfer effects [30].

In the literature, CDs for PEC water splitting have been mostly prepared by electrochemical etching of graphite [31–35] or by hydrothermal synthesis from organic compounds such as ascorbic acid [36], trinitropyrene [37], citric acid [38–40], ethylenediamine [41] and glucose/dicyandiamine [42]. Typically, the CD/TiO_2 composite is treated under hydrothermal conditions to improve the interaction between CDs and nanostructured TiO_2. Alternatively, the CD/TiO_2 photoanode can be prepared by immersion or electrochemical impregnation of the TiO_2 layer in the CD solution [33–35,39,40,43]. The PEC hydrogen generation with CD/TiO_2 photocatalysts has been performed in neutral (e.g. 0.5 M Na_2SO_4) or alkaline (1 M KOH) electrolytes. Therefore, previous works indicate that CDs improve the TiO_2 activity on PEC water splitting (Table 1). However, the large number of CD structures and possible electrode configurations suggest that other suitable combinations are still to be found.

It is apparent that both charge transport in the composite solid phase and reactions taking place in the solid-electrolyte interphase are complex and difficult to elucidate. Typically, the proposed mechanisms for the improvement of photocatalytic water splitting on CD/TiO_2 electrodes include sensitization, a fast electron transfer, effects of CD fluorescence and others. Several works have evidenced sensitization from CDs to TiO_2 under visible light, with fast transfer of excited electrons from the LUMO level of the CD to the conduction band of TiO_2 [31,32,34,36,39–41,43,51]. This mechanism for water splitting operates in other CD/semiconductor electrodes such as CD/Fe_2O_3 [52], CD/ZnO [53] and CD/WO_3 [54]. However, electron transfer from TiO_2 to the CD seems to be also possible, particularly under UV irradiation [32,36]. Other research works more specifically remark the CD effect of improving charge separation efficiency and decreasing the electron transport resistance [33,37,44].

Even though CDs can be prepared by a number of techniques and protocols, all of them have a greatly rich surface chemistry with a variety of functional groups containing oxygen, nitrogen and sulfur. Similarly to other carbon materials, nitrogen and sulfur doping in CDs has been related to the activity as co-catalyst in the cathode for electrochemical hydrogen evolution [55]. In addition, it has been reported that amino groups can active mechanisms of electron transfer to CDs during the photocatalytic hydrogen evolution [56]. In TiO_2 photoanodes, the role of the nitrogen doping level in hydrothermally synthesized CDs has been evidenced on both the photocatalytic hydrogen evolution and PEC water splitting [47,49,57]. A positive effect may also result from the co-sensitization of TiO_2 with CDs and Eosin Y dye [48]. However, the functionalization of CDs with specific chemical groups has been seldom explored for photocatalytic and PEC applications, in particular for hydrogen generation and water splitting. Also, problems with the long term stability of CDs have been detected by several authors [41], which need to be considered for practical application.

A novelty in the present work is the direct comparison of CDs that were prepared by different polycondensation and chemical functionalization methods, resulting in various structures and compositions. Polycondensation reactions were performed under microwave irradiation, hydrothermal conditions or by room-temperature solution chemistry with a coupling agent. Furthermore, CDs were functionalized with different chemical groups on their surface through the reaction with nucleophilic amines. The CDs were deposited on TiO_2 electrodes, which were used both in perovskite solar cells and as photoanodes for PEC water splitting. A substantial increase in the photocurrent of PEC water splitting was measured on the photoanode that was modified with chemically functionalized CDs. It was confirmed that the system is stable under continuous PEC operation. The PEC measurements, as well as the comparison with photovoltaic results, indicate that the improvement in the water oxidation efficiency takes place through a sensitization mechanism, in which both the TiO_2 and CDs act as semiconductors, while all the excited photoelectrons flow through TiO_2 to the collector.

Experimental

Synthesis of CDs

Three types of carbon nanoparticles, here labelled as MW-CDs, HS-CDs and But-CDs, are formed by polycondensation between citric acid and ethylenediamine and thus have a common basic polymeric structural unit (Fig. 1a). The MW-

Table 1 – Review of literature on PEC water splitting by CD/TiO_2 under full spectrum simulated solar light, indicating the achieved photocurrent density (J_{ph}, mA·cm^{-2}), the improvement with respect to the electrode without CDs, and the PEC measurement medium.

Photocatalyst[a]	CD synthesis (precursor)	J_{ph}	Improvement	Medium	Ref.
CQD/TiO_2 NT	Electrochemical (graphite)	1.0	x 4	0.25 M Na_2S, 0.35 M Na_2SO_3	[31]
CQD/TiO_2	Electrochemical (graphite)	1.2	x 4.8	0.25 M Na_2S, 0.35 M Na_2SO_3	[39]
CD/TNRA	Autoclave (citric acid, ethylenediamine)	0.35	x 1.2	0.01 M Na_2S, 0.1 M Na_2SO_4,	[41]
CQD/P25	Electrochemical (graphite)	0.5	x 2.5	1 M Na_2SO_4	[32]
CD/TiO_2 NW	Autoclave (ascorbic acid)	$0.24 \cdot 10^{-3}$	x 3	–	[36]
CD/TiO_2	Hydrothermal (citric acid, tridecanediamine)	0.4	x 2	1 M KOH	[43]
CD/TiO_2 NT	Autoclave (spinach)	$3.5 \cdot 10^{-3}$	x 2.3	–	[44]
GQD/TiO_2 NW	Oxidative chemical (graphite)	0.18	x 1.5	0.5 M Na_2SO_4	[45]
GQD/TiO_2	Oxidative chemical (graphite)	1.7	x 2.1	0.1 M Na_2SO_4	[46]
GQD/(001)TiO_2	Autoclave (trinitropyrene)	$0.9 \cdot 10^{-3}$	x 2.2	0.5 M Na_2SO_4	[37]
NHCS/TiO_2	Chemical vapor deposition (toluene, acetonitrile)	0.15	x 2.4	0.5 M H_2SO_4	[47]
CD/TiO_2 NT	Electrochemical (graphite)	0.37	x 1.2	1 M KOH	[33]
CD/TiO_2 NP	Electrochemical (graphite)	0.04	x 1.3	1 M KOH	[33]
CD/Eosin TiO_2 NT	Electrochemical (graphite)	0.49	x 1.5	TEOA, 0.5 M Na_2SO_4	[48]
NCQD/P25	Autoclave (ammonium citrate, ethylenediamine)	0.89	x 4	1 M Na_2SO_4	[49]
CQD/TiO_2 NR	Hydrothermal (citric acid)	2.51	x 1.9–4	0.1 M NaOH	[40]
CQD/H-TNRA	Autoclave (ascorbic acid)	3	x 1.5–6	1 M KOH	[50]

[a] Abbreviations: CQD = carbon quantum dot; NT = nanotube; TNRA = TiO_2 nanorod arrays; P25 = Aeroxide® P25 TiO_2; NW = nanowire; GQD = graphene quantum dot; NHCS = nitrogen doped hollow carbon sphere; NP = nanoparticle; NCQD = nitrogen doped CQD; NR = nanorod.

CDs are synthetized in a microwave system (CEM Discover SP reactor working in the open-batch modality) at a controlled temperature, while HS-CDs and But-CDs are synthetized in solution at room temperature, employing a coupling agent. Another important difference concerns the functionalization

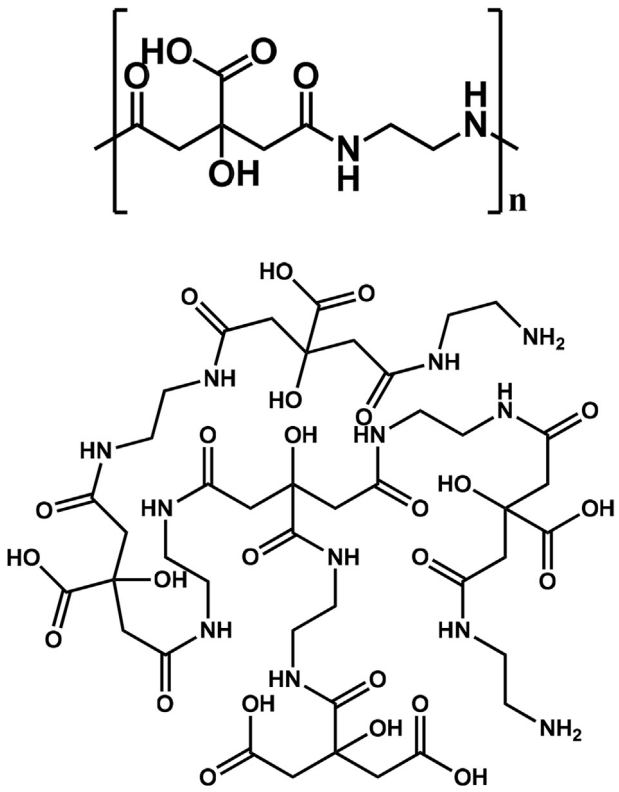

Fig. 1 – Top) chemical structure of a linear polymer that results from the polycondensation between citric acid and ethylenediamine; bottom) model structure of the polymer MW-CDs.

type: MW-CDs are synthesized only with citric acid and ethylenediamine and the resulting polymer structure resembles the one in Fig. 1b, where the functional groups are carboxylic acids, amines and alcohols [58]. In the synthesis of HS-CDs and But-CDs, one more step, which is a final addition of a nucleophilic amine, produces an additional functionalization. Specifically, the carboxylic acids of CDs react with the added amine, namely cysteamine for HS-CDs and butyl amine for But-CDs. Therefore, carboxylic acids are partially consumed and a new functional group is attached on the polymer structure, i.e. butyl-in But-CDs and thiol in HS-CDs [59]. In addition, primary amines from ethylenediamine and alcohols are still present. A hydrothermal process was used for the synthesis of a fourth type of CDs, which is named o-PDA-CDs. The structure of o-PDA-CDs is completely different, since the only reagent is *o*-phenylenediamine. Most probably, the amine group reacts with the aromatic ring, resulting in a completely conjugated polyaromatic structure, while the other CDs are non-conjugated.

For MW-CDs, citric acid monohydrate (2.0 g, 9.5 mmol) was dissolved in ultrapure water (16 mL). Upon the addition of ethylenediamine (0.64 mL, 9.5 mmol), the solution was heated through microwave irradiation. The mixture was irradiated to keep the temperature at 140 °C for 6 min and then the irradiation was stopped, yielding a yellow, transparent, solid product that was highly soluble in water. The product was dissolved in ultrapure water and dialyzed against ultrapure water (MWCO = 0.5–1.0 KDa, 3 days, twice a day). Dry MW-CDs were obtained by freeze-drying with a mass yield of 22 wt%.

For But-CDs, 300 mg of anhydrous citric acid (1.6 mmol, 1 equiv.) was dissolved in 4.0 ml of DMF. The solution was cooled in an ice bath and 0.73 ml of diisopropyl carbodiimide (DIC, 3 equiv.) was added. Subsequently, 105 μl of ethylenediamine (1 equiv.) in 4 ml of water was added and the mixture was stirred for 10 min at room temperature, while it

changed its color from slightly yellow to orange. Afterwards, 0.62 ml of n-butylamine (4 equiv.) in 4 ml of water was poured into the mixture, and it was stirred for 1 h. The crude was diluted in ultrapure water, filtrated on paper filter and washed with ethyl acetate for 2 times and dichloromethane for 2 times. Finally, the water phase was adjusted to pH = 7 with a diluited HCl solution and dialyzed against ultrapure water (MWCO = 0.5–1.0 KDa, 4 days, twice a day). After filtration on a 0.22 μm pore-size filter, water was removed by freeze-drying, obtaining 250 mg of product.

For HS-CDs, the procedure was nearly identical to that for the preparation of But-CDs. Instead of the addition of n-butylamine, 480 mg of cysteamine (4 equiv.) was added. The crude was not washed with dichloromethane, but just 3 times with ethyl acetate. After filtration and freeze-drying, 160 mg of product was obtained.

For o-PDA-CDs, *o*-phenylenediamine (0.8 g) was dissolved in water (8 mL) and treated in an autoclave at 200 °C for 4 h. Purification was performed by filtration through 3 μm and 0.22 μm filters. The remaining water was removed by vacuum drying. The solid was dispersed again in THF and dried.

Electrode preparation

Fluorinated tin oxide (FTO) substrates (Nippon Sheet Glass. 10 Ω/sq) were etched with Zn powder and 4 M HCl. Next, they were cleaned with Hellmanex®, acetone and ethanol, respectively for 15 min, inside an ultrasonic bath, and they were immediately blown with dry air. The compact TiO_2 (c-TiO_2) solution was prepared with titanium diisopropoxide bis(acetylacetonate): acetylacetone: ethanol at 0.6: 0.4: 9 vol ratio and it was sprayed onto FTO substrates at 450 °C. The mesoporous TiO_2 (m-TiO_2) paste was prepared mixing a commercial titanium paste (Dyesol, now Greatcell) with ethanol at 1:6 wt ratio; it was spin-coated onto the c-TiO_2 layer at 5000 rpm for 20 s and then it was dried at 80 °C for 5 min. The CD suspension (500 μL) was spin-coated onto FTO/c-TiO_2/m-TiO_2 substrates at 3000 rpm for 30 s, and then it was annealed at 450 °C on a hot plate in air for 30 min.

Characterization techniques

Elemental analysis (O, C, H, N, S) was performed in a Thermo Flash 1112 analyzer. Fourier-transform infrared (IR) spectroscopy was performed in a Bruker Vertex 70 spectrometer, on powder samples that were pressed into pellets with KBr. UV/Vis absorption spectra were recorded in a Shimadzu UV-2401 PC spectrophotometer. Photoluminescence excitation and emission spectra were recorded in a Horiba Jobin Yvon Fluoromax-P. All the spectra were recorded at room temperature using a 10 mm path-length quartz cuvette.

Scanning electron microscopy (SEM) was performed in a SEM-EDX Hitachi S-3400 N provided with a Si EDX analyser Röntec XFlash. High resolution images were taken in a MERLIN™ Carl Zeiss FESEM microscope. Micro-Raman spectra were obtained by means of a HORIBA Jobin Yvon Raman spectrometer HR 800UV. The spectra were acquired with a green laser at 532 nm under the 50x objective. X-ray photoelectron spectroscopy (XPS) measurements were acquired with an ESCAPlus spectrometer using the Al anode. Contact angle measurements were carried out by the sessile drop method in an Attension Optical Tensiometer by Biolin Scientific.

Perovskite solar cell fabrication and assessment

The quadruple cation halide perovskite $Rb_{0.05}Cs_{0.05}MA_{0.15}FA_{0.75}Pb_{1.05}(I_{0.89}Br_{0.11})_3$ was prepared by mixing PbI_2 (1.5 M), $PbBr_2$ (1.5 M), CsI (1.5 M), RbI (1.5 M), MAI and MABr in DMF:DMSO mixed solvent (4:1). The perovskite spin coating process was carried out at 2000 rpm for 10 s, and then 6000 rpm for 30s in a dry air glove box. During the second step of spin coating, 100 μL of chlorobenzene was injected at 15s before ending. Samples were annealed at 100 °C for 1 h on a hot plate for crystallization. The hole transporting layer was prepared by dissolving 0.12 g of spiro-OMeTAD in 1130 μL of chlorobenzene and then doping with 47.3 μL of TBP and 23.5 μL of TFSI (1.8 M in acetonitrile). The spin coating was conducted at 4000 rpm for 20 s. The finished devices were placed inside a dry air box for 12 h to fully oxidize the spiro-OMeTAD. Finally, 80 nm of Au was deposited as the back electrode by thermal evaporation.

The solar cells were measured using a 450 W Xenon light source (Oriel) equipped with an arc lamp housing (Newport, Model 66902, 50–500 W). The light intensity was calibrated with a Si photodiode equipped with an infrared cutoff filter (KG3, Schott), and was recorded during each measurement. The I–V curves were measured using a digital source meter (Keithley 2400) with a voltage scan rate of 10 mV/s and an active area of 0.16 cm^2. All the measurements were conducted in air at room temperature.

PEC water splitting

The PEC measurements were performed in a three electrode cell provided with a quartz window, using an AUTOLAB PGSTAT302 N. A graphite rod purchased from CYMIT Quimica was used as the counter electrode. Illumination was carried out using a 150 W Xe arc lamp by LOT-Oriel GmbH (irradiation power of 300 mW cm^{-2}), which simulates the solar spectrum in the ultraviolet and visible regions.

A reference electrode of Hg/HgO, 0.1 M KOH ($E^\circ = 0.165$ V vs. SHE) was utilized for the experiments. A nitrogen purge was utilized to avoid interferences of the oxygen reduction reaction. Experiments were performed in 0.1 M NaOH. Three electrochemical tests were performed: cyclic voltammetry (CV), potentiostatic photocurrent and open circuit potential measurements.

For cyclic voltammetry, the scan rate was of 20 mV s^{-1}. Several cycles were performed to detect the possible presence of irreversible phenomena. As a general observation, no changes were observed in CV after the fourth cycle and thus it is the one presented here. For voltammetry under irradiation, light was applied continuously during the whole cycle.

For photocurrent measurements under potentiostatic conditions, a bias potential of −0.037 V (vs. Hg/HgO, 0.1 M KOH) at pH 13 was applied, which respectively corresponds to the maximum voltage values in the cyclic voltammogram. Intermittent irradiation and dark periods of 15 s were applied during 5 min. Stability chronoamperograms were recorded at

−0.280 V. For the open circuit potential measurements at zero current, the cell was allowed to stabilize under dark conditions, and then the electrode was illuminated for 45 s. The photopotential (V_{ph}) was calculated as the difference between illumination and dark voltages.

Incident photon to current efficiency (IPCE) was measured under identical conditions to potentiostatic photocurrent experiments using a LOT Oriel monochromator (MSH-300).

Results and discussion

Characterization of CDs

The elemental analysis of the CDs is presented in Fig. 2a. The MW-CD nanoparticles contain approximately 45 wt% of carbon, as well as oxygen and nitrogen as heteroatoms. The HS-CDs show a certain quantity of sulfur, corresponding to thiol groups, together with a decrease in the oxygen with respect to MW-CDs. The But-CDs show an increase in the carbon ratio and a decrease in the oxygen, which support the success of the preparation by functionalization of MW-CDs with butyl chains. The o-PDA-CDs are mostly composed by carbon, nitrogen and hydrogen, but does not contain oxygen.

The IR spectra are presented in Fig. 2b. The signals confirm the expected functional groups for the different CD types [60]. The MW-CDs show clear features related to alcohol/phenol at around 3400, 3260 and 1440-1390 cm^{-1}, C=O stretching of carboxylic acids at 1700 cm^{-1}, vibrational modes I and II of amides at 1650 and 1560 cm^{-1}, and other oxygen and nitrogen groups in the range of 1190–1000 cm^{-1}. The HS-CDs show features similar to the MW-CDs, while differing in the intensity of the carboxylic acid stretching, which is strongly reduced as a consequence of the thiol functionalization. The But-CDs present the features of oxygen and nitrogen groups too; however, methylene bands in the range of 2970–2870 cm^{-1} are particularly relevant, and signals at 1200-1000 cm^{-1} are weak, which is consistent with the presence of butyl chains instead of certain oxygen groups.

The complete structural characterization of CDs that are synthesized by polycondensation reactions has been discussed previously [58,61]. The generic structure of polymer

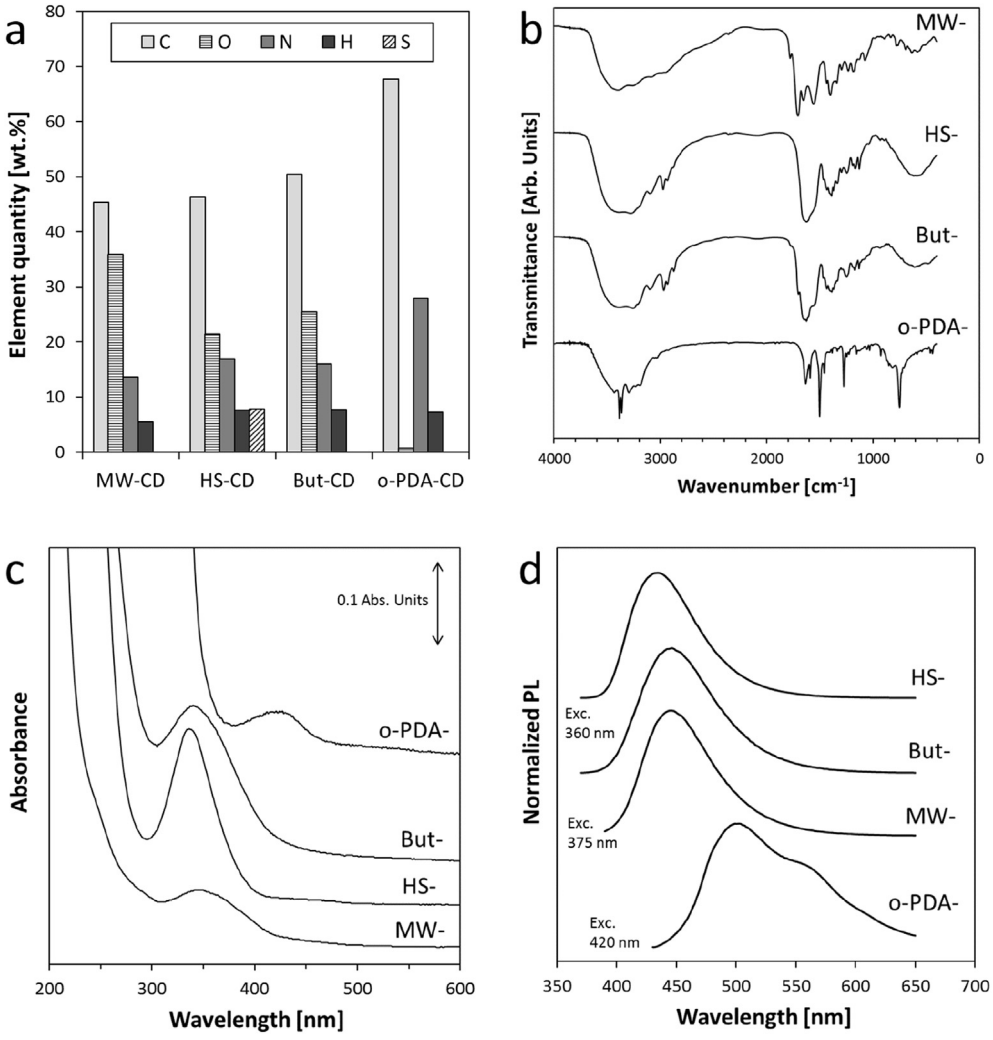

Fig. 2 – Characterization of the different CD types: a) elemental analysis, b) IR spectra, c) UV–Vis absorbance spectra, and d) PL emission spectra.

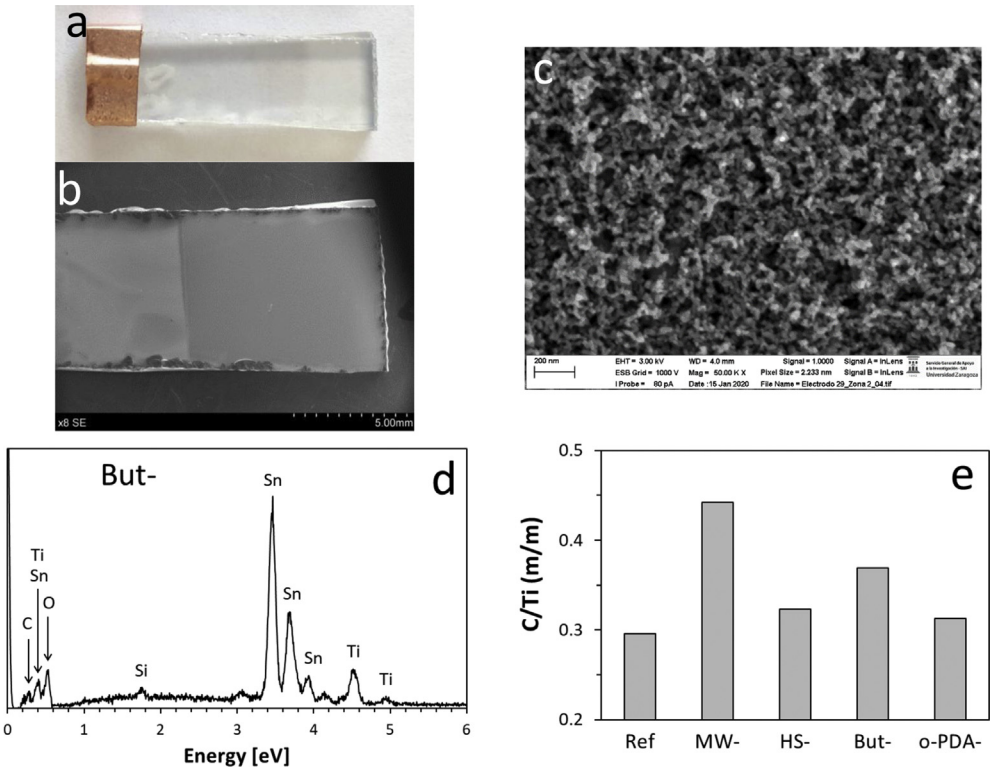

Fig. 3 – Characterization of c-TiO_2/m-TiO_2 + CD electrodes by SEM-EDX: a) picture of the electrode, b) image of the electrode by SEM, c) high resolution SEM image, d) EDX spectrum, and e) C/Ti mass ratio of the reference c-TiO_2/m-TiO_2 and electrodes with different types of CDs.

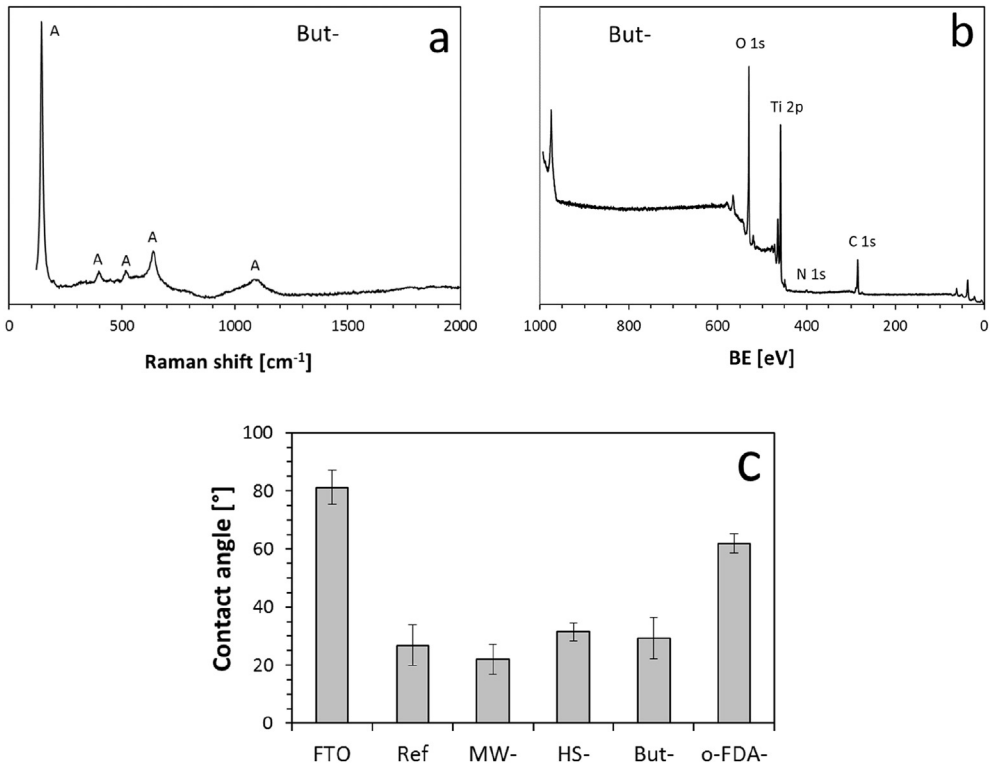

Fig. 4 – Characterization of c-TiO_2/m-TiO_2 + CD electrodes: a) Raman, b) XPS, and c) static contact angle measurements with pure water on the reference c-TiO_2/m-TiO_2 and electrodes with different types of CDs.

CDs, as it is depicted in Fig. 1, does not include carbon double bonds, and thus they do not contain graphene structures. The structural origin of fluorescence emission in polymer CDs has been considered in previous works [58,61]. Optical properties of CDs are presented in Fig. 2c (absorbance) and 2d (fluorescence). Spectra of MW-, HS- and But-CDs show intense light absorption in the UV region ($\lambda < 300$ nm) and an additional maximum at around 350 nm. In o-PDA-CDs, the intense continuous absorption extends to 350 nm, while the additional maximum shifts to around 420 nm. Emission spectra of MW-, HS- and But-CDs show maxima at 446, 434 and 446 nm respectively. The emission band of o-PDA-CDs has two clear contributions with maxima at 499 and around 560 nm.

Electrode characterization

The characterization of c-TiO_2/m-TiO_2 + CD electrodes was performed by SEM-EDX (Fig. 3), Raman spectroscopy, XPS and contact angle measurements (Fig. 4). The EDX analysis covers an electrode area in the range of a mm^2, thus being well representative of the electrode composition. The analysis depth reaches the Sn from the FTO substrate. The reference c-TiO_2/m-TiO_2 electrode contains adventitious carbon, while all the electrodes with CDs present increased quantities of carbon in its composition. High resolution SEM images reveal the mesoporous structure of the electrode surface, which is given by the aggregation of TiO_2 crystals. Raman spectra indicate that TiO_2 on the electrodes is mostly in the anatase phase, while it might contain only very small quantities of rutile. The phase composition of TiO_2 does not suffer changes upon the addition of CDs. Similarly, the XPS analysis does not detect substantial changes in the chemical environment of titanium with the deposition of CDs. Contact angle measurements with pure water reveal an increase in the hydrophobic character of the TiO_2 surface after the deposition of o-PDA-CDs; the other functionalized CDs do not induce changes with respect to the reference TiO_2 electrode.

Perovskite solar cells

Fig. 5 presents a configuration schematic and the results of perovskite solar cells. The perovskite active material was infiltrated on the c-TiO_2/m-TiO_2 + CD region, according to the schematic in Fig. 5. Typical IV plots were obtained and the characteristic cell parameters were calculated. The results are in good agreement with previous works under similar cell configurations [62,63]. Statistically, the photoconversion efficiency (PCE) is kept with the deposition of CDs on the TiO_2 electrode, and remains around 17% (Fig. 5d). Similarly, other characteristic parameters remain nearly unchanged

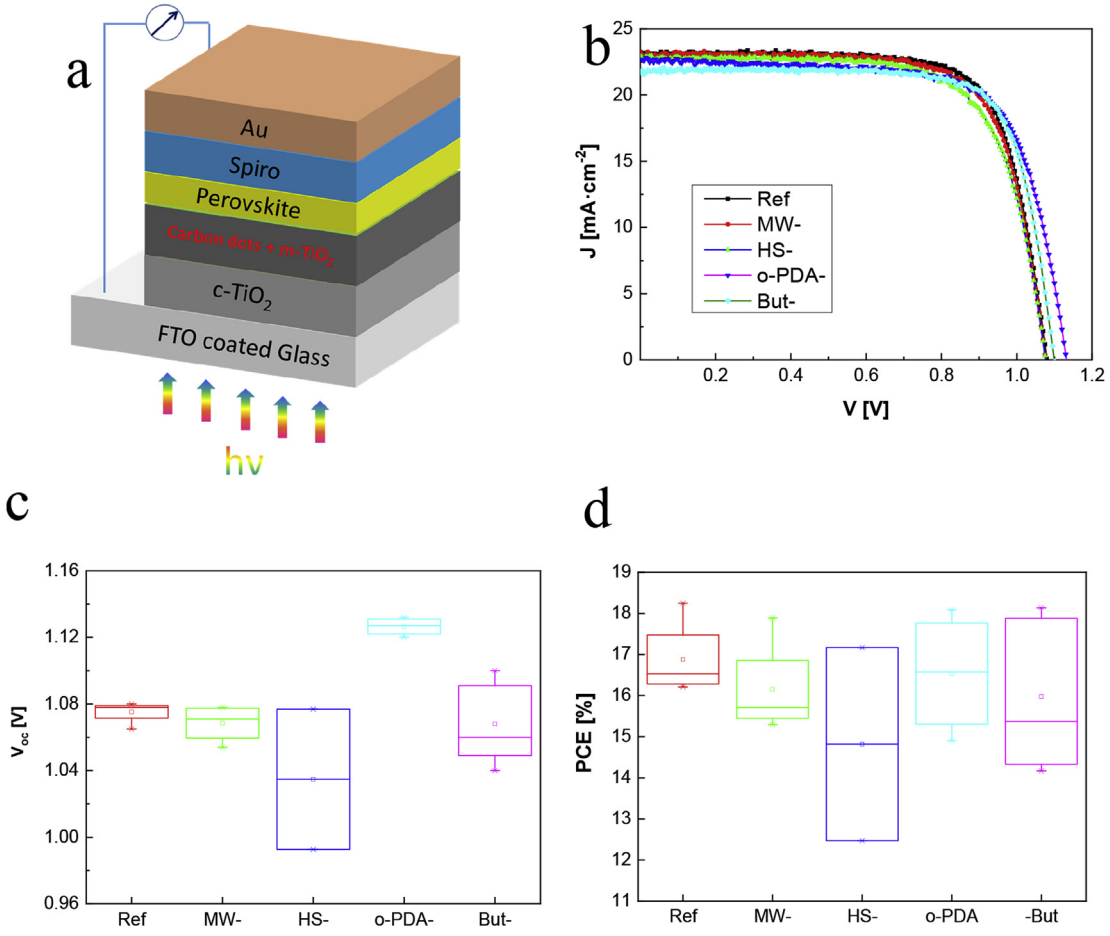

Fig. 5 – Schematic configuration and characterization of perovskite solar cells: a) schematic explaining the cell layer components; b) IV curves; c) V_{OC}; and d) PCE statistics for the reference c-TiO_2/m-TiO_2 and electrodes bearing different functionalized CDs (four solar cells for each type were measured).

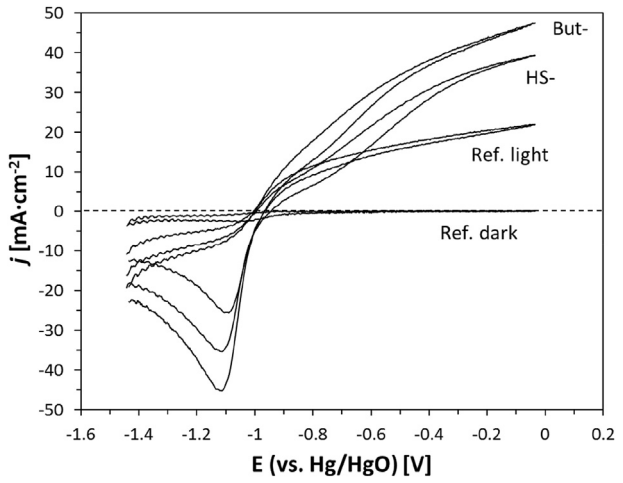

Fig. 6 – CV analysis of the reference c-TiO_2/m-TiO_2 electrode (dark and light conditions) and electrodes bearing HS- and But-CDs under irradiation.

(J_{SC} ~ 22 mA/cm^2; FF ~ 0.7%). Interestingly, the open circuit voltage (V_{OC}) experiences a substantial increase with the deposition of o-PDA-CDs. This change in V_{OC} has to be associated to differential characteristics of o-PDA-CDs. First of all, their composition and structure are different from the other CDs, in particular the high nitrogen ratio and the absence of oxygen. As a consequence, the contact angle of the c-TiO_2/m-TiO_2 + But-CD surface increases, indicating an increase in the hydrophobic character. Since the perovskite is infiltrated as an organic solution in the cell, the hydrophobic character might improve the structural characteristics or interactions of perovskite crystals. Secondly, the optical absorbance and photoluminescence properties of the o-PDA-CDs are also substantially different, suggesting particular optical and electronic responses. Recent works on perovskite cells have underlined the positive effect of N-doping in graphene quantum dots to improve their properties against humidity, temperature stress and UV irradiation, as well as a hole transport material [64,65]. In the present work, it is further observed that CDs containing only nitrogen as a heteroatom, but not oxygen, exhibit improved interface properties in perovskite solar cells.

PEC water splitting

The results of PEC water oxidation are presented in Figs. 6–9. The cyclic voltammetry experiment (Fig. 6) on the reference c-TiO_2/m-TiO_2 electrode shows an anodic photocurrent at E > −1 V (vs. Hg/HgO). This photocurrent has to be strictly related to water oxidation with evolution of O_2 in the working electrode, and thus to H_2 evolution in the counter electrode. The deposition of CDs on the reference c-TiO_2/m-TiO_2 electrode provides an increase in the photocurrent, particularly in the case of But-CDs. The photocurrent in the modified electrode reaches nearly 2.3 times that of the c-TiO_2/m-TiO_2 electrode. Even though photocurrent densities are low, the improvement that was caused by CDs well agrees with previous literature data (Table 1). Apart from photocurrents, other voltammetry characteristics, such as the onset potentials at around −1 V (vs. Hg/HgO) and the presence of Wilson states in the cathodic scan at around −1.1 V (vs. Hg/HgO) [23] are not modified by the CDs, indicating that the general mechanism of the reaction is unchanged.

Amperometric experiments at E > −1 V were conducted to evaluate the kinetics of the system response and the long term stability (Fig. 7). It is confirmed that the deposition of But-CDs substantially improves the photocurrent without altering the speed in the response. In addition, the c-TiO_2/m-TiO_2 + But-CD system is stable for more than 4 h under continuous operation in PEC water splitting. All the CD-modified electrodes, at equivalent working potentials of E > −1 V (vs. Hg/HgO), produce higher photocurrents than the reference TiO_2 electrode. However, the photopotential, calculated from open circuit voltages (j = 0), does not show substantial changes (Fig. 8). This fact, in agreement with observations on cyclic voltammograms, indicates that no substantial changes are introduced by CDs in the reaction mechanism on the TiO_2 electrode. In addition, this agrees with the results in perovskite cells, which indicate few changes in the electron transport properties.

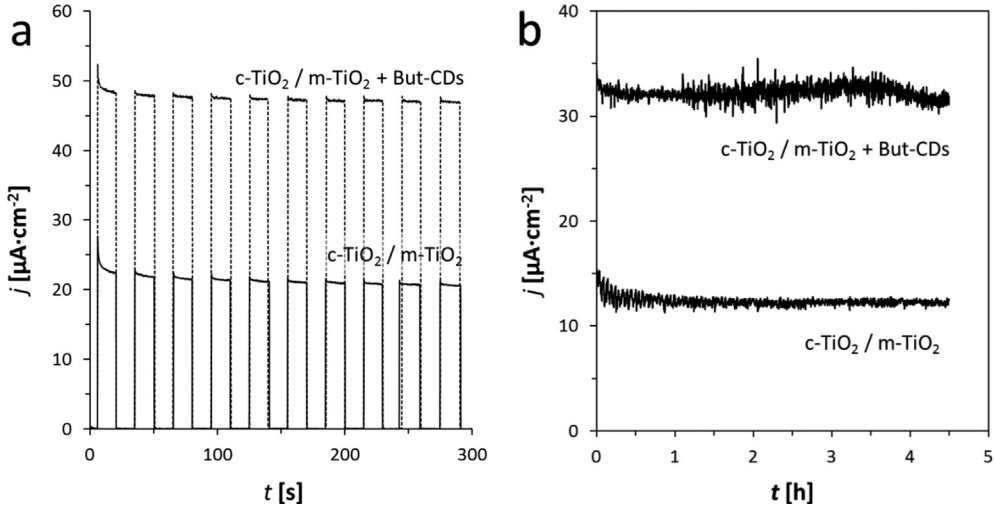

Fig. 7 – Photocurrent measurements under potentiostatic conditions: a) On/off irradiation at −0.037 V vs. Hg/HgO; b) continuous illumination at −0.280 V vs. Hg/HgO.

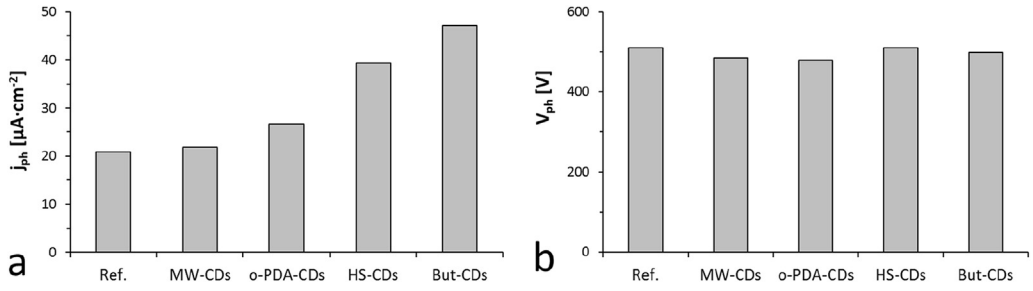

Fig. 8 – Parameters of PEC water oxidation on the reference c-TiO_2/m-TiO_2 and electrodes bearing different functionalized CDs: a) potentiostatic photocurrent at −0.037 V vs. Hg/HgO; b) photopotential.

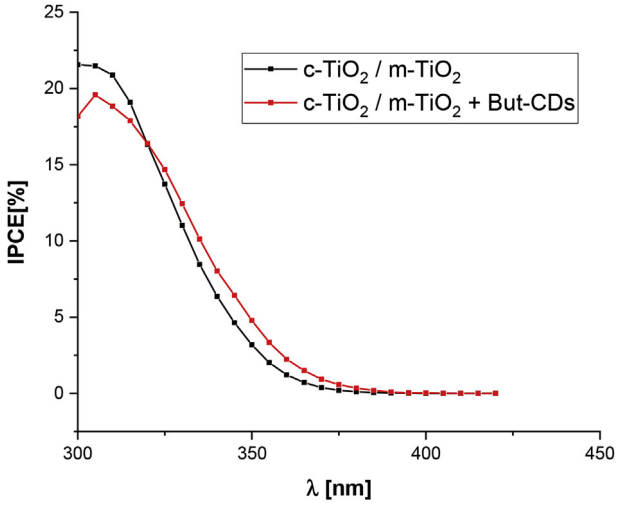

Fig. 9 – IPCE measurement on the reference c-TiO_2/m-TiO_2 and the modified c-TiO_2/m-TiO_2 + But-CDs electrode in 0.1 M NaOH at −0.037 V (vs. Hg/HgO).

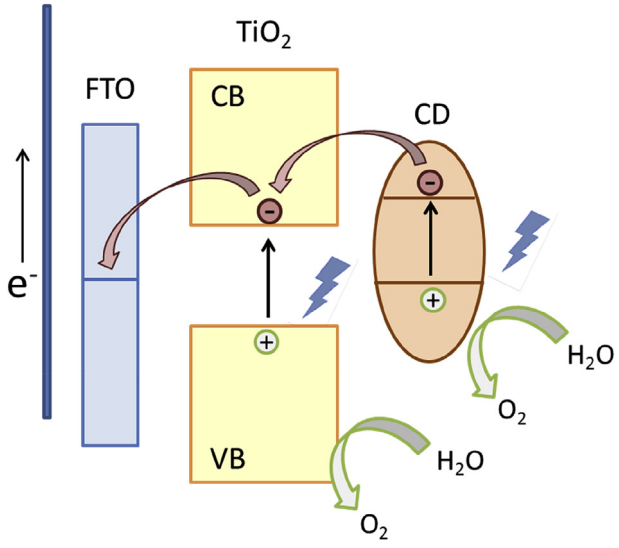

Fig. 10 – Schematic explaining the mechanism of PEC water oxidation on modified c-TiO_2/m-TiO_2 + CD electrodes: both the TiO_2 and CDs work as semiconductors; all the photoexcited electrons flow through the TiO_2 layer (CB = conduction band; VB = valence band).

Fig. 9 shows the conversion efficiency as a function of the incident irradiation wavelength. The outcomes prove that the CD-modified electrode has a higher efficiency than the reference TiO_2 electrode at larger irradiation wavelengths. The light absorption range is extended by approximately 20 nm. Therefore, the increase in the photocurrent can be associated with a contribution of a light harvesting path through the CD, which acts as a sensitizer (Fig. 10). Both the TiO_2 and CDs are simultaneously working as semiconductors, absorbing photons and pumping excited photoelectrons, while the photoholes react oxidizing water. The CDs provide an equivalent bandgap somewhat narrower than TiO_2. However, all the photoelectron paths seem to be flowing through TiO_2, since onset potentials and photopotentials for the process are not modified. As a consequence, it is deduced that the LUMO level of the CD is located at a higher energy than the lowest active level of the TiO_2 conduction band, in agreement with previous findings on TiO_2 nanotubes loaded with graphene quantum dots [45]. Functional groups on the CD might modulate the energy levels to achieve the most suitable interaction with TiO_2.

Conclusions

Various types of fluorescent CDs with different functional groups were synthesized from simple organic acids and amines by microwave irradiation, hydrothermal treatment, solution chemistry with coupling agents and chemical functionalization with nucleophilic amines. The CDs were deposited on thin film c-TiO_2/m-TiO_2 electrodes; a comparison was performed using analogous electrodes as anode components in perovskite photovoltaic cells and as active photoanodes in PEC water splitting. In perovskite solar cells, an increase in V_{OC} occurs upon deposition of o-PDA-CDs, which has to be associated to their particular properties: a high nitrogen ratio, absence of oxygen, increased hydrophobic character and different optical behavior. The PEC water oxidation, in terms of photocurrent, improves upon CD deposition, and the increment depends on functionalization. The highest photocurrents were measured on c-TiO_2/m-TiO_2 + But-CD electrodes, which are proved to be stable under continuous operation. All the PEC experiments, and particularly the IPCE, demonstrate that CDs work as sensitizers of TiO_2. The CDs act themselves as semiconductors that increase the optical

absorption range by approximately 20 nm, thus increasing the current flow through TiO_2.

Acknowledgements

This work has been funded by the Spanish MINEICO under the project ENE 2016-79282-C5-1-R (AEI/FEDER, UE), the Government of Aragón (Grupo reconocido T03-17R) and associated EU Regional Development Funds (DGA/FEDER, UE). Special thanks are directed to the Analysis Service at Instituto de Carboquímica ICB-CSIC.

REFERENCES

[1] Ni M, Leung M, Leung D, Sumathy K. A review and recent developments in photocatalytic water-splitting using TiO2 for hydrogen production. Renew Sustain Energy Rev 2007;11(3):401–25.
[2] Pagliaro M, Palmisano G, Ciriminna R, Loddo V. Nanochemistry aspects of titania in dye-sensitized solar cells. Energy Environ Sci 2009;2(8):838–44.
[3] Schneider J, Matsuoka M, Takeuchi M, Zhang J, Horiuchi Y, Anpo M, Bahnemann D. Understanding TiO_2 photocatalysis: mechanisms and materials. Chem Rev 2014;114(19):9919–86.
[4] Bai Y, Mora-Sero I, De Angelis F, Bisquert J, Wang P. Titanium dioxide nanomaterials for photovoltaic applications. Chem Rev 2014;114(19):10095–130.
[5] Zhen C, Wu T, Chen R, Wang L, Liu G, Cheng H. Strategies for modifying TiO_2 based electron transport layers to boost perovskite solar cells. ACS Sustainable Chem Eng 2019;7(5):4586–618.
[6] Singh R, Dutta S. A review on H-2 production through photocatalytic reactions using TiO_2/TiO_2-assisted catalysts. Fuel 2018;220:607–20.
[7] Jian J, Jiang G, van de Krol R, Wei B, Wang H. Recent advances in rational engineering of multinary semiconductors for photoelectrochemical hydrogen generation. Nano Energy 2018;51:457–80.
[8] Cecconi B, Manfredi N, Montini T, Fornasiero P, Abbotto A. Dye-sensitized solar hydrogen production: the emerging role of metal-free organic sensitizers. Eur J Org Chem 2016;31:5194–215.
[9] Zhou W, Li W, Wang J, Qu Y, Yang Y, Xie Y, Zhang K, Wang L, Fu H, Zhao D. Ordered mesoporous black TiO_2 as highly efficient hydrogen evolution photocatalyst. J Am Chem Soc 2014;136(26):9280–3.
[10] Zhang W, He H, Tian Y, Lan K, Liu Q, Wang C, Liu Y, Elzatahry A, Che R, Li W, Zhao D. Synthesis of uniform ordered mesoporous TiO_2 microspheres with controllable phase junctions for efficient solar water splitting. Chem Sci 2019;10(6):1664–70.
[11] El Rouby W, Antuch M, You S, Beaunier P, Millet P. Novel nano-architectured water splitting photoanodes based on TiO_2 -nanorod mats surface sensitized by ZIF-67 coatings. Int J Hydrogen Energy 2019;44(59):30949–64.
[12] Li W, Elzatahry A, Aldhayan D, Zhao D. Core-shell structured titanium dioxide nanomaterials for solar energy utilization. Chem Soc Rev 2018;47(22):8203–37.
[13] Treekamol Y, Schieda M, Herrmann-Geppert I, Klassen T. Optimized photoactive coatings prepared with functionalized TiO_2. Int J Hydrogen Energy 2019;44(60):31800–7.
[14] Zhang W, He H, Tian Y, Li H, Lan K, Zu L, Xia Y, Duan L, Li W, Zhao D. Defect-engineering of mesoporous TiO2 microspheres with phase junctions for efficient visible-light driven fuel production. Nano Energy 2019;66:104113.
[15] Fauet T, Keller V, Cottineau T, El Khakani M. Enhanced visible-light-photoconversion efficiency of TiO_2 nanotubes decorated by pulsed laser deposited CoNi nanoparticles. Int J Hydrogen Energy 2019;44(54):28656–67.
[16] Hu J, Li Y, Zhang S, Zhang Q, Liu Y, Zuo J, Li Q, Peng F. MoS_2 supported on hydrogenated TiO_2 heterostructure film as photocathode for photoelectrochemical hydrogen production. Int J Hydrogen Energy 2019;44(59):31008–19.
[17] Hu G, Lei Y, Hu R, Sun H, Gu Q, Ren D, Wang H. Photoelectrocatalytic water oxidation based on an earth-abundant metallic semiconductor-molecule hybrid photoanode. Int J Hydrogen Energy 2019;44(60):31884–91.
[18] Ghobadi TGU, Ghobadi A, Karadas F, Ozbay E. Large scale compatible fabrication of gold capped titanium dioxide nanoantennas using a shadowing effect for photoelectrochemical water splitting. Int J Hydrogen Energy 2020;45:1521–31.
[19] Sun B, Zhou W, Li H, Ren L, Qiao P, Li W, Fu H. Synthesis of particulate hierarchical tandem heterojunctions toward optimized photocatalytic hydrogen production. Adv Mater 2018;30(43).
[20] Sajjadizadeh H-S, Goharshadi EK, Ahmadzadeh H. Photoelectrochemical water splitting by engineered multilayer TiO_2/GQDs photoanode with cascade charge transfer structure. Int J Hydrogen Energy 2020;45:123–34.
[21] Caudillo-Flores U, Kubacka A, Berestok T, Zhang T, Llorca J, Arbiol J, Cabot A, Fernández-García M. Hydrogen photogeneration using ternary $CuGaS_2$-TiO_2-Pt nanocomposites. Int J Hydrogen Energy 2020;45:1510–20.
[22] Yu J, Ma T, Liu S. Enhanced photocatalytic activity of mesoporous TiO_2 aggregates by embedding carbon nanotubes as electron-transfer channel. Phys Chem Chem Phys 2011;13(8):3491–501.
[23] Anson-Casaos A, Hernandez-Ferrer J, Rubio-Munoz C, Santidrian A, Teresa Martinez M, Benito AM, Maser WK. Electron trap states and photopotential of nanocrystalline titanium dioxide electrodes filled with single-walled carbon nanotubes. Chem Electro Chem 2017;4(9):2300–7.
[24] Ng B, Putri L, Tan L, Pasbakhsh P, Chai S. All-solid-state Z-scheme photocatalyst with carbon nanotubes as an electron mediator for hydrogen evolution under simulated solar light. Chem Eng J 2017;316:41–9.
[25] Olowoyo J, Kumar M, Jain S, Babalola J, Vorontsov A, Kumar U. Insights into reinforced photocatalytic activity of the CNT-TiO_2 nanocomposite for CO_2 reduction and water splitting. J Phys Chem C 2019;123(1):367–78.
[26] Kim H, Moon G, Monllor-Satoca D, Park Y, Choi W. Solar photoconversion using graphene/TiO_2 composites: nanographene shell on TiO_2 core versus TiO_2 nanoparticles on graphene sheet. J Phys Chem C 2012;116(1):1535–43.
[27] Zhang X, Sun Y, Cui X, Jiang Z. A green and facile synthesis of TiO_2/graphene nanocomposites and their photocatalytic activity for hydrogen evolution. Int J Hydrogen Energy 2012;37(1):811–5.
[28] Zhang X, Zhang B, Huang D, Yuan H, Wang M, Shen Y. TiO_2 nanotubes modified with electrochemically reduced graphene oxide for photoelectrochemical water splitting. Carbon 2014;80:591–8.
[29] Morais A, Longo C, Araujo J, Barroso M, Durrant J, Nogueira A. Nanocrystalline anatase TiO_2/reduced graphene oxide composite films as photoanodes for photoelectrochemical water splitting studies: the role of reduced graphene oxide. Phys Chem Chem Phys 2016;18(4):2608–16.

[30] Jin S, Kim D, Jun G, Hong S, Jeon S. Tuning the photoluminescence of graphene quantum dots through the charge transfer effect of functional groups. ACS Nano 2013;7(2):1239–45.
[31] Zhang X, Wang F, Huang H, Li H, Han X, Liu Y, Kang Z. Carbon quantum dot sensitized TiO_2 nanotube arrays for photoelectrochemical hydrogen generation under visible light. Nanoscale 2013;5(6):2274–8.
[32] Yu H, Zhao Y, Zhou C, Shang L, Peng Y, Cao Y, Wu L, Tung C, Zhang T. Carbon quantum dots/TiO_2 composites for efficient photocatalytic hydrogen evolution. J Mater Chem 2014;2(10):3344–51.
[33] Sang L, Lin J, Zhao Y. Preparation of carbon dots/TiO_2 electrodes and their photoelectrochemical activities for water splitting. Int J Hydrogen Energy 2017;42(17):12122–32.
[34] Wang Q, Huang J, Sun H, Zhang K, Lai Y. Uniform carbon dots@TiO_2 nanotube arrays with full spectrum wavelength light activation for efficient dye degradation and overall water splitting. Nanoscale 2017;9(41):16046–58.
[35] Zhang Y, Tian H, Zhao G. Enhanced visible-light photoelectrocatalytic activity of {001}TiO_2 electrodes assisted with carbon quantum dots. Chem Electro Chem 2015;2(11):1728–34.
[36] Wang J, Gao M, Ho G. Bidentate-complex-derived TiO_2/carbon dot photocatalysts: in situ synthesis, versatile heterostructures, and enhanced H_2 evolution. J Mater Chem 2014;2(16):5703–9.
[37] Yu S, Zhong Y, Yu B, Cai S, Wu L, Zhou Y. Graphene quantum dots to enhance the photocatalytic hydrogen evolution efficiency of anatase TiO_2 with exposed {001} facet. Phys Chem Chem Phys 2016;18(30):20338–44.
[38] Zhou Y, Yang S, Fan D, Reilly J, Zhang H, Yao W, Huang J. Carbon quantum dot/TiO_2 nanohybrids: efficient photocatalysts for hydrogen generation via intimate contact and efficient charge separation. ACS Applied Nano Materials 2019;2(2):1027–32.
[39] Yu X, Liu R, Zhang G, Cao H. Carbon quantum dots as novel sensitizers for photoelectrochemical solar hydrogen generation and their size-dependent effect. Nanotechnology 2013;24(33):335401.
[40] Feng M, Liu Y, Wei N, Ma S, Li Z, Li H, Chen S, Liu J, Wang D. Alumina anchored CQDs/TiO_2 nanorods by atomic layer deposition for efficient photoelectrochemical water splitting under solar light. J Mater Chem 2018;6(37):18293–303.
[41] Bian J, Huang C, Wang L, Hung T, Daoud W, Zhang R. Carbon dot loading and TiO_2 nanorod length dependence of photoelectrochemical properties in carbon dot/TiO_2 nanorod array nanocomposites. ACS Appl Mater Interfaces 2014;6(7):4883–90.
[42] Feng T, Zeng Q, Lu S, Yang M, Tao S, Chen Y, Zhao Y, Yang B. Morphological and interfacial engineering of cobalt-based electrocatalysts by carbon dots for enhanced water splitting. ACS Sustainable Chem Eng 2019;7(7):7047–57.
[43] Xie S, Su H, Wei W, Li M, Tong Y, Mao Z. Remarkable photoelectrochemical performance of carbon dots sensitized TiO_2 under visible light irradiation. J Mater Chem 2014;2(39):16365–8.
[44] Wang J, Ng Y, Lim Y, Ho G. Vegetable-extracted carbon dots and their nanocomposites for enhanced photocatalytic H_2 production. RSC Adv 2014;4(83):44117–23.
[45] Sudhagar P, Herraiz-Cardona I, Park H, Song T, Noh S, Gimenez S, Sero I, Fabregat-Santiago F, Bisquert J, Terashima C, Paik U, Kang Y, Fujishima A, Han T. Exploring graphene quantum dots/TiO_2 interface in photoelectrochemical reactions: solar to fuel conversion. Electrochim Acta 2016;187:249–55.
[46] Hao X, Jin Z, Xu J, Min S, Lu G. Functionalization of TiO_2 with graphene quantum dots for efficient photocatalytic hydrogen evolution. Superlattice Microst 2016;94:237–44.
[47] Ranganathan K, Morais A, Nongwe I, Longo C, Nogueira A, Coville N. Study of photoelectrochemical water splitting using composite films based on TiO_2 nanoparticles and nitrogen or boron doped hollow carbon spheres as photoanodes. J Mol Catal Chem 2016;422:165–74.
[48] Sang L, Lei L, Lin J, Ge H. Co-sensitization of TiO_2 electrode with Eosin Y dye and carbon dots for photoelectrochemical water splitting: the enhanced dye adsorption and the charge transfer route. Int J Hydrogen Energy 2017;42(50):29686–93.
[49] Shi R, Li Z, Yu H, Shang L, Zhou C, Waterhouse G, Wu L, Zhang T. Effect of nitrogen doping level on the performance of N-doped carbon quantum dot/TiO_2 composites for photocatalytic hydrogen evolution. Chem Sus Chem 2017;10(22):4650–6.
[50] Liang Z, Hou H, Fang Z, Gao F, Wang L, Chen D, Yang W. Hydrogenated TiO_2 nanorod arrays decorated with carbon quantum dots toward efficient photoelectrochemical water splitting. ACS Appl Mater Interfaces 2019;11(21):19167–75.
[51] Sargin I, Yanalak G, Arslan G, Patir I. Green synthesized carbon quantum dots as TiO_2 sensitizers for photocatalytic hydrogen evolution. Int J Hydrogen Energy 2019;44(39):21781–9.
[52] Xie X, Yang Y, Xiao Y, Huang X, Shi Q, Zhang W. Enhancement of photoelectrochemical activity of Fe_2O_3 nanowires decorated with carbon quantum dots. Int J Hydrogen Energy 2018;43(14):6954–62.
[53] Cammi D, Zimmermann K, Gorny R, Vogt A, Dissinger F, Gad A, Markiewcz N, Waag A, Prades J, Ronning C, Waldvogel S, Voss T. Enhancement of the sub-band-gap photoconductivity in ZnO nanowires through surface functionalization with carbon nanodots. J Phys Chem C 2018;122(3):1852–9.
[54] Shi W, Zhang X, Brillet J, Huang D, Li M, Wang M, Shen Y. Significant enhancement of the photoelectrochemical activity of WO_3 nanoflakes by carbon quantum dots decoration. Carbon 2016;105:387–93.
[55] Wang L, Wu X, Guo S, Han M, Zhou Y, Sun Y, Huang H, Liu Y, Kang Z. Mesoporous nitrogen, sulfur co-doped carbon dots/CoS hybrid as an efficient electrocatalyst for hydrogen evolution. J Mater Chem 2017;5(6):2717–23.
[56] Xu X, Bao Z, Zhou G, Zeng H, Hu J. Enriching Photoelectrons via three transition channels in amino conjugated carbon quantum dots to boost photocatalytic hydrogen generation. ACS Appl Mater Interfaces 2016;8(22):14118–24.
[57] Song T, Zhang X, Wei Y, Yang P. N-Cdots-decorated TiO_2(B)/anatase microspheres with high photocatalytic performance in visible light. Int J Hydrogen Energy 2019;44(59):31129–40.
[58] Vallan L, Urriolabeitia E, Ruiperez F, Matxain J, Canton-Vitoria R, Tagmatarchis N, Benito A, Maser W. Supramolecular-enhanced charge transfer within entangled polyamide chains as the origin of the universal blue fluorescence of polymer carbon dots. J Am Chem Soc 2018;140(40):12862–9.
[59] Vallan L, Urriolabeitia EP, Benito AM, Maser WK. A versatile room-temperature method for the preparation of customized fluorescent non-conjugated polymer dots. Polymer 2019;177:97–101.
[60] Coates J. Interpretation of Infrared spectra, a practical approach. In: Meyers RA, editor. Encyclopedia of analytical chemistry. Chichester: Wiley; 2000. p. 10815–37.

[61] Vallan L, Hernandez-Ferrer J, Grasa L, Gonzalez-Dominguez J, Martinez M, Ballesteros B, Urriolabeitia E, Anson-Casaos A, Benito A, Maser W. Differential properties and effects of fluorescent carbon nanoparticles towards intestinal theranostics. Colloids Surf B Biointerfaces 2020;185:110612.
[62] Li H, Shi W, Huang W, Yao E, Han J, Chen Z, Liu S, Shen Y, Wang M, Yang Y. Carbon quantum dots/TiOx electron transport layer boosts efficiency of planar heterojunction perovskite solar cells to 19%. Nano Lett 2017;17(4):2328–35.
[63] Sidhik S, Velusamy J, De la Rosa E, Perez-Garcia S, Ramos-Ortiz G, Lopez-Luke T. Role of carbon nanodots in defect passivation and photo-sensitization of mesoscopic-TiO_2 for perovskite solar cells. Carbon 2019;146:388–98.
[64] Bian H, Wang Q, Yang S, Yan C, Wang H, Liang L, Jin Z, Wang G, Liu S. Nitrogen-doped graphene quantum dots for 80% photoluminescence quantum yield for inorganic -$CsPbI_3$ perovskite solar cells with efficiency beyond 16%. J Mater Chem 2019;7(10):5740–7.
[65] Kang G, Lee S, Yeo J, Choi E, Lee D, Na S, Joh H. Graphene quantum dots with nitrogen and oxygen derived from simultaneous reaction of solvent as exfoliant and dopant. Chem Eng J 2019;372:624–30.